4429

Robust retrospective correction of 3D golden-ratio radial MRI using electromagnetic tracking

Tess E Wallace[1,2], Simon K Warfield[1,2], and Onur Afacan[1,2]

[1]Computational Radiology Laboratory, Boston Children's Hospital, Boston, MA, United States, [2]Harvard Medical School, Boston, MA, United States

Synopsis

Radial MRI is intrinsically more robust to motion than Cartesian sampling; however, if large rotational motion occurs, the uniform sampling of conventional 3D radial acquisitions is disrupted and is difficult to recover retrospectively. The golden angle ratio has been used to generate a quasi-isotropic distribution of spokes over time in 2D, but is limited to fully correct for motion, which occurs in three dimensions. Extending the flexibility of golden-ratio spoke ordering to 3D radial sampling, combined with rigid-body motion tracking using electromagnetic sensors, enables robust retrospective correction by maintaining relatively uniform sampling, even in the presence of large-amplitude rotational motion.

Purpose

Radial MRI acquisitions are intrinsically more robust to motion than Cartesian trajectories as the center of ***k***-space is densely oversampled and artifacts manifest as local blurring, rather than ghosting.[1] Measuring and correcting for motion using external tracking or self-navigated sub-sets of the projection data may be used to further improve image quality.[2] Conventional 3D radial sampling uses a linear or bit-reversed spoke ordering that traces out a spiral trajectory on the surface of a sphere. However, if rotational motion occurs, this sampling pattern is interrupted, resulting in “gaps” in the ***k***-space data, which are difficult to recover retrospectively (Fig. 1). The golden angle ratio has been widely used in 2D and pseudo-3D (“stack-of-stars”) radial imaging to generate a relatively isotropic distribution of spokes over the scan duration, enabling more flexible reconstruction algorithms.[3] However, 2D approaches are limited in their ability to fully correct for motion, which occurs in three dimensions. This flexibility may be extended to 3D radial sampling, using higher dimensional golden ratios derived from modified Fibonacci sequences.[4] In this work, we implement a 3D golden-ratio radial acquisition strategy that improves retrospective motion correction results compared to standard 3D radial and Cartesian acquisitions.

Methods

We modified a 3D radial pulse sequence to acquire ***k***-space data with a golden-ratio sampling scheme. The two-dimensional golden ratios $\phi_1 = 0.4656$ and $\phi_2 = 0.6823$ were used to increment the azimuthal and polar angles of each 3D radial projection, generating a set of spatially and temporally uniformly distributed spokes (Fig. 1).

Phantom experiment. An ACR phantom was scanned at 3T (Siemens, Erlangen, Germany) using a 3D GRE sequence with the following scan parameters: TR/TE = 7.4/2.4 ms, α = 6°, RBW = 400 Hz/pix, FOV = 220 mm, 1 mm^3 isotropic resolution, 48,000 spokes for radial acquisitions, acquisition time ~ 6 min. Five scans were acquired for each trajectory; the phantom was translated and rotated during scans two and four, respectively. Rigid-body motion measurements from four electromagnetic (EM) sensors (Robin Medical, Baltimore, MD) placed on the surface of the phantom were combined using singular value decomposition[5] and used to retrospectively correct the ***k***-space lines from each scan. Radial reconstruction was performed in Matlab (R2016b; MathWorks) by applying a weighting function computed using an iterative numerical approach[6] and regridding the data using the NUFFT toolbox.[7]

Volunteer experiment. Three volunteers were scanned at 3T after obtaining informed consent. An MPRAGE sequence was used to generate a T_1-weighted image with the following scan parameters: TR/TE/TI = 1540/2.77/800 ms, α = 5°, RBW = 300 Hz/pix, FOV = 256 mm, 1 mm^3 isotropic resolution, 48,000 spokes, acquisition time ~ 6.5 min. Three scans were acquired for each sampling trajectory with: 1) no motion; 2) six abrupt head movements; 3) slow continuous nodding. Reconstruction was performed as described above using EM tracking motion measurements to retrospectively correct the ***k***-space data. The normalized root-mean-square error (NRMSE) and structural similarity index (SSIM)[8] were computed relative to the ‘no motion’ scan. Mean motion scores[9] were also estimated for each scan to ensure head movements were comparable for each sampling trajectory.

Results

EM tracking successfully compensated for inter-scan motion in the phantom experiment. For intra-scan motion, residual artifacts are visible in both the corrected Cartesian and conventional radial scans, which are effectively removed by the golden-ratio sampling scheme (Fig. 2). Retrospective correction results for volunteers performing abrupt head movements (Fig. 3) and continuous nodding motion (Fig. 4) also demonstrate substantially improved image quality with the golden-ratio radial sampling. Across all volunteers and both motion paradigms, NRMSE following correction was 3.98 ± 0.59%, 3.99 ± 1.08% and 2.64 ± 0.49% for the Cartesian, radial and golden-ratio acquisitions, respectively. SSIM relative to the reference image was 0.78 ± 0.06, 0.80 ± 0.07 and 0.91 ± 0.03, for comparable levels of motion (Fig. 5).

Discussion

Combining EM tracking with a 3D golden-ratio sampling trajectory enabled robust retrospective correction by accurately compensating for the effects of translational and rotational motion, while maintaining a sufficiently dense sampling of ***k***-space. Conventional radial reconstruction did not demonstrate substantially improved results compared to Cartesian sampling. A further advantage of the golden-ratio ordering scheme is that its flexible self-navigating properties may also be used to correct the imaging data. Retrospectively corrected golden-ratio radial MPRAGE acquisitions provided comparable gray-white matter contrast to Cartesian MPRAGE and maintained excellent image quality, even in the presence of large head movements, making this a promising method for robust neuroanatomical imaging of young children and other challenging patient populations.

Acknowledgements

This research was supported in part by the following grants: NIH-5R01EB019483, NIH-4R01NS079788 and NIH-R44MH086984.

References

1. Kecskemeti, S. et al. Robust Motion Correction Strategy for Structural MRI in Unsedated Children Demonstrated with 3D Radial MPnRAGE. ***Radiology*** (ahead of print) (2018). doi:10.1148/radiol.2018180180

2. Anderson, A., Velikina, J., Block, W., Wieben, O. & Samsonov, A. Adaptive retrospective correction of motion artifacts in cranial MRI with multi-coil 3D radial acquisitions. ***Magn. Reson. Med.*** **69**, 1094–1103 (2014).

3. Block, K. T. et al. Towards Routine Clinical Use of Radial Stack-of-Stars 3D Gradient-Echo Sequences for Reducing Motion Sensitivity. ***J. Korean Soc. Magn. Reson. Med.*** **18**, 87-106 (2014).

4. Chan, R. W., Ramsay, E. A., Cunningham, C. H. & Plewes, D. B. Temporal stability of adaptive 3D radial MRI using multidimensional golden means. ***Magn. Reson. Med.*** **61**, 354–363 (2009).

5. Umeyama, S. Least-Squares Estimation of Transformation Parameters Between Two Point Patterns. ***IEEE Trans. Pattern Anal. Mach. Intell.*** **13**, 376–380 (1991).

6. Pipe, J. G. & Menon, P. Sampling density compensation in MRI: rationale and an iterative numerical solution. ***J. Magn. Reson. Imaging*** **41**, 179–186 (1999).

7. Fessler, J. A. Michigan Image Reconstruction Toolbox. Available at: https://web.eecs.umich.edu/~fessler/code/. (Accessed: 1st June 2017)

8. Wang, Z., Bovik, A. C., Sheikh, H. R. & Simoncelli, E. P. Image quality assessment: From error visibility to structural similarity. ***IEEE Trans. Image Process.*** **13**, 600–612 (2004).

9. Tisdall, M. D. et al. Volumetric navigators for prospective motion correction and selective reacquisition in neuroanatomical MRI. ***Magn. Reson. Med.*** **68**, 389–399 (2012).

Figures

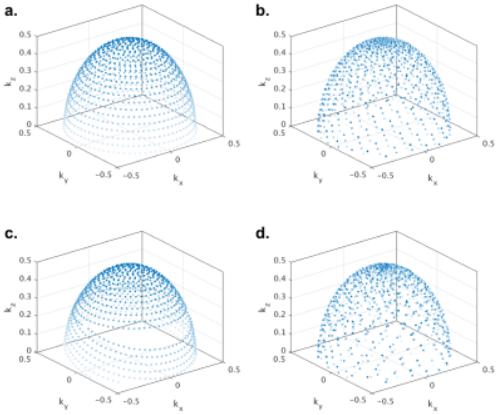

Figure 1. ***k***-Space trajectories for conventional 3D radial sampling (a) and golden-ratio 3D radial sampling (b), simulated for 1000 spokes. Simulated 10° rotation around the y-axis causes a 'gap' in the conventional radial k-space trajectory (c), while the golden-ratio trajectory retains a more uniform spatiotemporal sampling pattern (d).

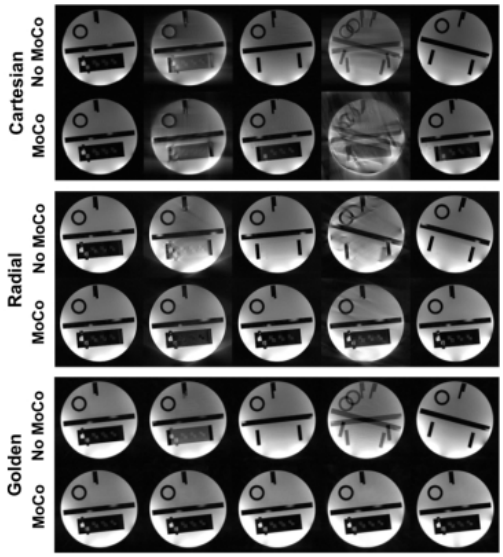

Figure 2. Comparison of retrospective correction of inter- and intra-scan motion in an ACR phantom with 3D Cartesian, conventional radial and golden-ratio radial sampling trajectories. Large intra-scan translation and rotation resulted in residual artifacts in both retrospectively corrected Cartesian and conventional radial scans, which are not present with the golden-ratio sampling scheme.

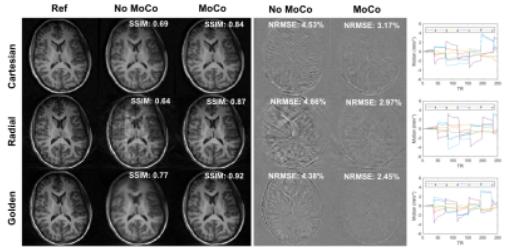

Figure 3. Axial slice through 3D Cartesian, conventional radial and golden-ratio radial scans and difference images relative to the 'no motion' scan for abrupt motion, before and after retrospective correction with EM tracking motion measurements (right). Golden-ratio radial sampling enables robust retrospective motion correction, resulting in the highest image quality metrics.

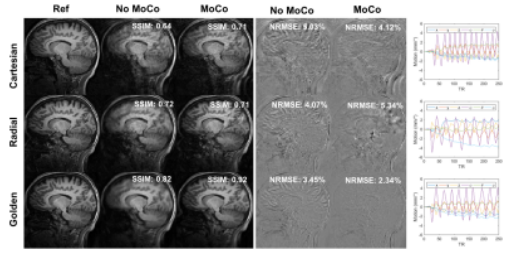

Figure 4. Sagittal slice through 3D Cartesian, conventional radial and golden-ratio radial scans and difference images relative to the 'no motion' scan for continuous nodding, before and after retrospective correction with EM tracking motion measurements (right). Residual artifacts are present in both the Cartesian and conventional radial corrected images, while golden-ratio radial sampling enables highest-quality images, even in the presence of large, continuous motion.

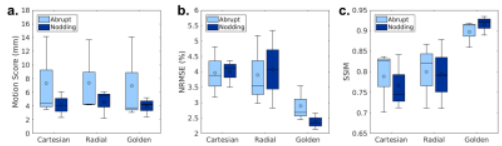

Figure 5. Boxplots showing mean motion score in mm (a), normalized root-mean-square error (NRMSE) in percent (b) and structural similarity index (SSIM) (c) after retrospective motion correction for 3D Cartesian, conventional radial and golden-ratio radial sampling in three volunteers performing abrupt head movements and continuous nodding motion. Motion scores were comparable across all sampling trajectories; 3D golden-ratio radial sampling enables substantially higher image quality following retrospective correction for both types of motion.

Proc. Intl. Soc. Mag. Reson. Med. 27 (2019)
4429